Lab on a Chip

PAPER

View Article Online
View Journal | View Issue



Cite this: *Lab Chip*, 2023, **23**, 2057

# Compressive molding of engineered tissues *via* thermoresponsive hydrogel devices†

Camille Cassel de Camps, ‡[a] Stephanie Mok, ‡[b] Emily Ashby,[b] Chen Li,[b] Paula Lépine,[c] Thomas M. Durcan[c] and Christopher Moraes *[abde]

Received 4th January 2023,
Accepted 3rd March 2023

DOI: 10.1039/d3lc00007a

rsc.li/loc

Biofabrication of tissues requires sourcing appropriate combinations of cells, and then arranging those cells into a functionally-useful construct. Recently, organoids with diverse cell populations have shown great promise as building blocks from which to assemble more complex structures. However, organoids typically adopt spherical or uncontrolled morphologies, which intrinsically limit the tissue structures that can be produced using this bioassembly technique. Here, we develop microfabricated smart hydrogel platforms in thermoresponsive poly(*N*-isopropylacrylamide) to compressively mold microtissues such as spheroids or organoids into customized forms, on demand. These Compressive Hydrogel Molders (CHyMs) compact at cell culture temperatures to force loaded tissues into a new shape, and then expand to release the tissues for downstream applications. As a first demonstration, breast cancer spheroids were biaxially compacted in cylindrical cavities, and uniaxially compacted in rectangular ones. Spheroid shape changes persisted after the tissues were released from the CHyMs. We then demonstrate long-term molding of spherical brain organoids in ring-shaped CHyMs over one week. Fused bridges formed only when brain organoids were encased in Matrigel, and the resulting ring-shaped organoids expressed tissue markers that correspond with expected differentiation profiles. These results demonstrate that tissues differentiate appropriately even during long-term molding in a CHyM. This platform hence provides a new tool to shape pre-made tissues as desired, *via* temporary compression and release, allowing an exploration of alternative organoid geometries as building blocks for bioassembly applications.



## Introduction

Biofabrication aims to create 3D tissue constructs with living cells, for a variety of applications,[1,2] and generally requires microscale strategies to organize and position multiple cell types with respect to each other, as well as macroscale approaches to shape the overall tissue. Traditional biofabrication techniques first form a biomaterial scaffold, and then populate the scaffold by seeding with cells.[1,3] Bioprinting has recently gained traction in constructing engineered tissues,[1,3] in which cells and matrix material are simultaneously positioned in a layer-by-layer fashion to produce a complex 3D structure.[4,5] However, real tissues and organs are typically much more dense, functionally-diverse, and finely-organized at the microscale[4,6,7] than can be achieved with conventional bioprinting approaches.[4,7] Furthermore, appropriate sources for the wide variety of cells required in most tissues remains a major limitation.

Organoid cultures, differentiated from pluripotent stem cells in a 3D matrix, have emerged as a potential strategy to obtain multiple finely-organized and functional cell types, but differing culture protocols and media formulation requirements often limit their ability to recreate an entire organ system, particularly those with specialized and distinct components. Assembling disparate organoids into a larger tissue *via* bioprinting may resolve this issue,[4,6] while addressing the limitations of each technique: organoids offer high cell density, realistic cell types and local architectures,[7–9] while bioprinting can integrate and assemble functional tissue units to recreate organ function.[6] This approach has recently been used to create a continuous intestinal tube with various gut cells,[10] perfusable tissue

[a] *Department of Biomedical Engineering, McGill University, Montréal, H3A 2B4 QC, Canada. E-mail: chris.moraes@mcgill.ca*
[b] *Department of Chemical Engineering, McGill University, Montréal, H3A 0C5 QC, Canada*
[c] *Early Drug Discovery Unit (EDDU), Montreal Neurological Institute and Hospital, McGill University, 3801 University Street, Montréal, H3A 2B4 QC, Canada*
[d] *Rosalind and Morris Goodman Cancer Institute, McGill University, Montréal, H3A 1A3 QC, Canada*
[e] *Division of Experimental Medicine, McGill University, Montréal, H4A 3J1, QC, Canada*

† Electronic supplementary information (ESI) available. See DOI: https://doi.org/10.1039/d3lc00007a

‡ These authors contributed equally.

aggregates,[7] and physiologically realistic mammary[11] and neural structures.[12,13] These successes collectively demonstrate that hybrid multi-scale engineering of organoids and assembly *via* bioprinting or positioning is a promising strategy to reconstruct and study developmental processes *in vitro*, in more complex models than can be achieved with single-type organoids.[14]

A potential limitation in this hybrid approach is that the shape of the building block organoid is largely uncontrolled, which in turn limits the tissue patterns that can be created. While some techniques have been developed to influence organoid shape,[15–17] these strategies either leave embedded structures within the tissues, or will require modification of existing culture protocols which may unexpectedly affect organoid function. Here, we envision a strategy in which an organoid generated with current protocols can be compressively molded into a desired shape on demand, before being released for downstream processing in bioprinting applications. However, molding an organoid into an arbitrary shape presents significant challenges in mechanical design, as the molding structure must reversibly actuate with multiple spatially patterned degrees of freedom and movement. Furthermore, the molding process must create sufficient force to permanently deform the organoid, allow release of the soft biological tissue from the mold, and maintain viability and cell function during and after operation.

To address these challenges, we turned to smart hydrogels that can be formed in specific geometries, and adopt distinct morphologies[18–21] in response to various environmental triggers.[20–24] Poly(*N*-isopropylacrylamide) (PNIPAM) is a well-established material that contracts at temperatures above ~32 °C,[25] and can maintain a contracted shape at cell culture temperatures. Here, we develop a strategy to fabricate Compressive Hydrogel Molders (CHyMs; Fig. 1A) in PNIPAM that can apply controlled strains to engineered tissues in culture. Tissues can be released on demand by cooling the cultures to room temperature. We demonstrate the utility of this platform using breast cancer spheroids and brain organoids, and show (1) that applied strains are sufficient to compact spheroids and change their shape, and (2) that a model organoid system can be formed into ring-like structures while maintaining their expected differentiation program in long-term CHyM culture.

## Methods

Unless otherwise stated, all cell culture materials and supplies were purchased from Fisher Scientific (Ottawa, ON), and chemicals were from Sigma-Aldrich (Oakville, ON).

### Device fabrication & characterization

Assembled mold chambers consisted of several pieces to allow for complete disassembly after casting to easily remove the hydrogel devices. Mold pieces for the CHyM microcavities were designed in Fusion 360 and printed on an AutoDesk Ember STL 3D printer using PR-57 K black

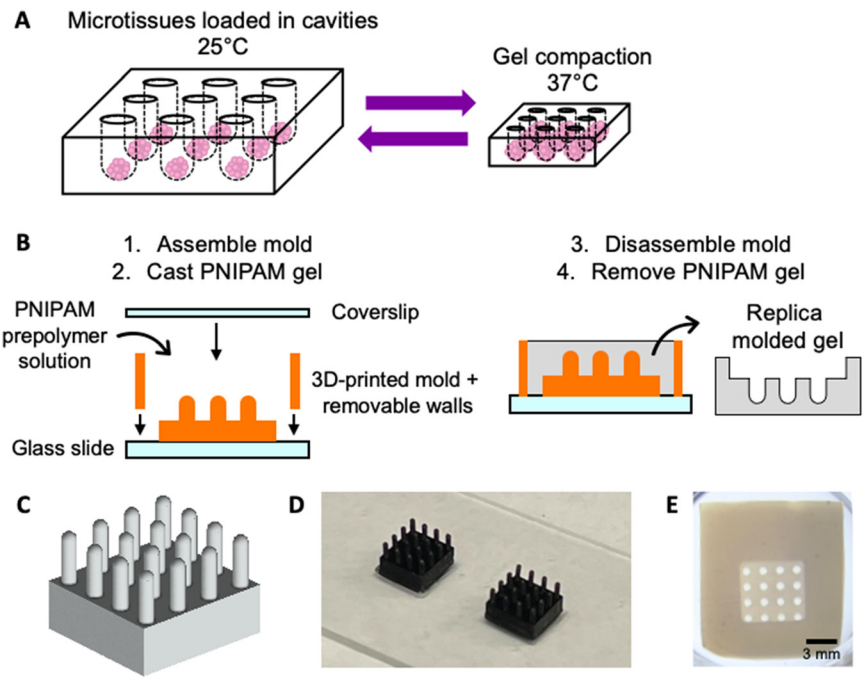


Fig. 1 Compressive hydrogel molder (CHyM) fabrication. A Schematic of microtissue compression in temperature-actuated PNIPAM hydrogel devices. B Mold pieces are 3D printed in-house with microcavity geometries as desired, assembled for PNIPAM hydrogel casting, and disassembled to release replica molded gel devices. C Mold design, D 3D printed microcavity molds glued to glass slide, and E replica molded CHyM with circular microcavities.

 

resin (Colorado Photopolymer Solutions) with 10 μm layer thickness. Molds were washed in isopropanol, and cured overnight in a UV chamber at 36 W. Mold walls were designed in AutoCAD and printed in PLA filament on a Monoprice Select Mini V2 printer. CHyM mold pieces were glued onto glass slides using Gorilla Super Glue to form the bottom of the mold, and mold walls were fastened to the glass slide (Fig. 1A). Separate solutions of 1% (w/v) ammonium persulfate (APS) in phosphate-buffered saline (PBS) and PNIPAM pre-gel (consisting of 1215 μL 20% PNIPAM in PBS, 810 μL 2% bis-acrylamide, 405 μL PBS, and 4 μL TEMED per slide) were prepared in glass test tubes and purged of oxygen by bubbling nitrogen gas through the liquid for 20 minutes, as described previously.[26] The two solutions were mixed in a 1 : 9 ratio (APS solution to PNIPAM pre-gel), poured into the assembled mold, and a glass coverslip was placed on top to limit oxygen diffusion into the polymerizing hydrogel for 20 minutes. To facilitate casting of the small central pillars in the ring-shaped CHyMs, 70% ethanol was sprayed onto the mold before filling, and a syringe and needle (25 gauge) were used to fill the pillars. The mold was disassembled to release the PNIPAM CHyMs, which were trimmed using a razor blade, rinsed in water, and then washed 3 times in PBS. CHyMs were allowed to swell overnight in 1% antibiotic–antimycotic in PBS, and stored in this solution at 4 °C until use. To reduce cell adhesion to contracted PNIPAM (which is hydrophobic), CHyMs were incubated in a filtered solution of 1% BSA in PBS for 2 hours at 37 °C the day before spheroid/organoid loading. They were kept in this solution overnight at 4 °C, rinsed with PBS, and soaked in media for 2 hours at room temperature immediately before use.

### Spheroid & organoid generation

All cell cultures were maintained at 37 °C with 5% $CO_2$. Human breast cancer cell line T47D (ATCC HTB-133) was maintained in Dulbecco's Modified Eagle Medium with 10% fetal bovine serum and 1% antibiotic–antimycotic (complete media) with media changes every 2–3 days, and passaged using 0.25% trypsin–EDTA when 80% confluent. Spheroids were generated as previously described,[27] using a polyacrylamide (PAA) micropocket platform to aggregate T47D cells. Briefly, cell suspensions were prepared at $15 \times 10^6$ cells per mL, dispensed into PAA devices, and incubated for 2 days to allow spheroid formation before loading into CHyMs. Spheroids were also generated in agarose micropockets, with the same method. The agarose micropockets were fabricated using micropocket mold pieces (3D printed as above) in PNIPAM mold assemblies. A 1% agarose solution was microwaved in 10 second intervals until melted, used to fill the mold assemblies, and then allowed to set for 40 minutes. Agarose devices were prepared for cell culture in the same manner as CHyMs.

iPSCs were cultured in mTeSR (StemCell Technologies) on Matrigel-coated plates with daily media changes, and passaged using Gentle Cell Dissociation Reagent (StemCell Technologies) when 70% confluent. Regions of spontaneous differentiation were cleared manually. The use of iPSCs in this research was approved by the McGill University Health Centre Research Ethics Board (DURCAN_IPSC/2019-5374). Cerebral organoids were generated according to the Lancaster protocol[8] using human control iPSC line AIW002-02 (male), which was obtained through The Neuro's C-BIG repository and had passed multistep quality control.[28] Cells that were at least 70% confluent were washed with DMEM and incubated with Accutase (Gibco) for 3–5 minutes. DMEM (equal volume to Accutase) was added, the liquid pipetted across the surface of the culture vessel to assist with detaching the cells, and collected; this was repeated once more. Cells were centrifuged at 1200 rpm for 3 minutes. The pellet was resuspended in 1 mL of hES media (low bFGF, with ROCK inhibitor; consisting of 400 mL DMEM-F12 + Glutamax, 100 mL Knockout Serum Replacement, 15 mL hESC-quality FBS (Gibco), 5 mL MEM-non-essential amino acids, 3.5 μL 2-mercaptoethanol, bFGF at 4 ng $mL^{-1}$ final concentration, and ROCK inhibitor at 50 μM final concentration)[8] using a P1000 tip plus a P200 tip on top.[29] An aliquot was stained with Trypan Blue, and cells were counted using a LUNA-II™ Automated Cell Counter. Cell suspensions were diluted in hES media to seed 10 000 live cells/well in 96-well round-bottom ultralow attachment plates (Corning Costar), and centrifuged at 1200 rpm for 10 minutes. Media was changed on Day 2 to hES media (low bFGF, no ROCK inhibitor), on Day 4 to hES media (no bFGF, no ROCK inhibitor), and on Day 6 to neural induction media (consisting of DMEM-F12 + Glutamax, 1% N2 supplement, 1% MEM-non-essential amino acids, and heparin at 1 μg $mL^{-1}$ final concentration)[8] using a multichannel pipette. To remove media, the culture plate was held vertically so organoids would fall to the sides of the wells; pipette tips were inserted into the wells at an upwards angle, away from the organoids, and media was aspirated slowly. To add media, the culture plate was rested on a surface horizontally, and pipette tips were inserted into the wells at an angle so that they pressed against the sides of the wells; media was ejected slowly. Organoids were maintained until Day 10 in neural induction media before loading into CHyMs.

### Tissue compression in CHyMs & release

To remove spheroids from the PAA micropockets so they could be loaded into CHyMs, media was pipetted rapidly at the micropocket device to displace the spheroids. In a separate plate, media was aspirated out of wells and CHyM microcavities, and cut P200 pipette tips (tips were cut to enlarge the opening) were used to transfer spheroids or early-stage organoids into the devices. Tissues were allowed to settle into the microcavities for several minutes before adding media to each well (complete media for T47D spheroids, neural induction media for cerebral organoids).

Devices were incubated at 37 °C for up to 2 weeks with media changes every 4 days. Matrigel was added to some organoids the day after loading by pipetting a droplet onto the ring microcavity. To release tissues from CHyMs after compressive molding, media was removed from the wells and cold media was added to quickly drop the temperature of the devices to expand them and allow for tissue removal, after which tissues were returned to 37 °C.

### Live tissue analyses

Spheroids and organoids were imaged using an EVOS™ M700 Imaging System or an Olympus IX73 spinning disc confocal microscope. Live/dead staining was performed using calcein AM and ethidium homodimer-1 (Life Technologies) at 4 μM in media for 40 minutes at 37 °C. Device and tissue measurements were performed manually in Fiji software,[30] using the Stitching plugin[31] where necessary to stitch image tiles together.

### Immunostaining

Tissues were fixed with 4% (w/v) paraformaldehyde, spheroids overnight at 4 °C, and organoids for 1 hour at room temperature with CHyMs flipped upside down, and then washed 3 times with PBS. Organoids were stained using a whole-mount staining protocol. They were blocked for 4 hours at room temperature with 0.5% Triton X-100 + 5% goat serum in PBS, and incubated with primary antibodies diluted in blocking buffer overnight at 4 °C. Organoids were then washed 3 times for 10 minutes in PBS, incubated with secondary antibodies and Hoescht 33342 diluted in blocking buffer overnight at 4 °C, and washed 3 times. Early-stage brain organoids were mounted on glass slides with Fluoromount Aqueous Mounting Media, coverslips were sealed with clear nail polish, and images were collected on a Zeiss laser scanning confocal microscope. Organoids compressed in CHyMs were imaged with a Leica TCS SP8 confocal microscope using an imaging chamber created by a stack of adhesive imaging spacers (Electron Microscopy Sciences, 70327-8S) between a glass slide and coverslip. Antibodies and stains were used as follows: anti-N-cadherin at 1 : 25 (rat monoclonal, DSHB Hybridoma Product MNCD2; MNCD2 was deposited to the DSHB by Takeichi, M./Matsunami, H.), anti-E-cadherin at 1 : 200 (rabbit monoclonal, Abcam ab40772), anti-E-cadherin at 1 : 50 (mouse monoclonal, Abcam ab1416), goat anti-rat IgG (H + L) Alexa Fluor® 555 at 1 : 500 (polyclonal, Life Technologies A21434), donkey anti-rabbit IgG H&L (DyLight® 650) at 1 : 500 (polyclonal, Abcam ab96894), goat anti-mouse IgG H&L (Alexa Fluor® 488) at 1 : 1000 (polyclonal, Abcam ab150113), phalloidin–tetramethylrhodamine B isothiocyanate at 1 : 50 (Sigma-Aldrich P1951), and Hoescht 33342 at 1 : 5000 (Invitrogen H3570).

### Statistical analysis

Analyses were performed in R statistical software.[32] If data were normally distributed and variances were equal, one-way ANOVA was performed with Tukey *post hoc* comparisons; if variances were not equal, Welch's *t*-test was performed for 2 groups, or Welch's ANOVA for more groups with Games–Howell *post hoc* tests. If data were non-normally distributed, the Wilcoxon signed-rank test was performed for 2 groups, or the Kruskal–Wallis test was performed for more groups. For paired data, as the differences of the pairs were not normally distributed, the Wilcoxon matched-pairs signed-rank test was used. All analyses for significance were carried out with $\alpha = 0.05$.

## Results & discussion

### CHyM device fabrication

To produce the temperature-actuated CHyMs needed to compress tissues (Fig. 1A), PNIPAM hydrogels were cast against and released from stereolithographically-printed 3D molds (Fig. 1B–D), which we have previously used to produce complex shapes for tissue engineering in polyacrylamide hydrogels.[27] This approach allowed us to rapidly iterate and design a wide variety of geometries, and to incorporate sloped walls above the microcavity to funnel the cultured tissue into the cavity. Replica molded PNIPAM gels released easily from the disassembled polymerization chamber (Fig. 1E), and were confirmed to contract at temperatures above ~32 °C. When placed in a 37 °C incubator, devices rapidly contracted, but expansion of the contracted hydrogels when returned to room temperature was slower and took up to 2 hours to swell completely, depending on device geometry. Fortunately, the initial expansion was generally sufficient to release compressed tissues within minutes, and expansion can be accelerated by adding chilled media, provided the biological tissue can handle the cold shock without long-term impact.

### Directionally-defined compressive molding

To demonstrate the potential for this technology in applying multidirectional strains to tissues of interest, we developed two simple test cases in which tissues can be biaxially compacted in a cylindrical microcavity, or uniaxially compressed between platens in a rectangular microcavity (Fig. 2A). With this formulation of PNIPAM, hydrogels reproduced mold features with reasonable fidelity, and cavity shapes were observed to shrink to less than half their original size upon incubation (Fig. 2B). Although some warping was observed at the CHyM periphery (likely due to manual trimming of the devices during fabrication), the tissue chamber features themselves shrank evenly with no skew or stretch, and shrinkage was highly consistent and predictable (Fig. 2C and D). Since it may be possible to alter the degree of compaction based on gel formulation, we tested other PNIPAM pre-gel formulations with varying concentrations of PNIPAM. Device contraction was found to be significantly impacted, but over a relatively small

 

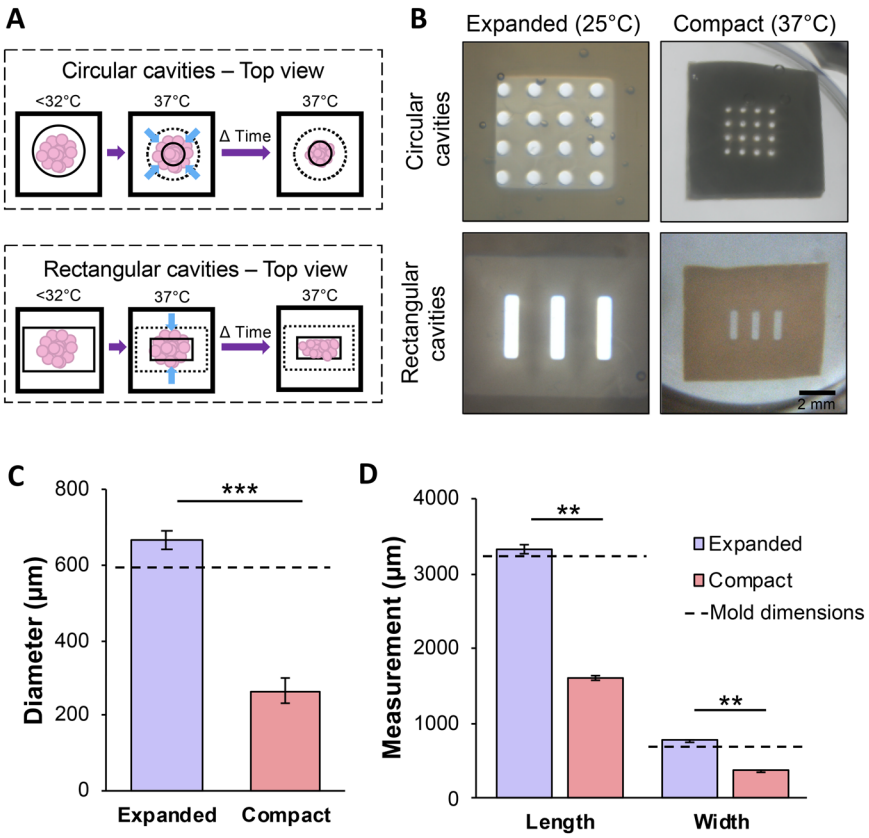


**Fig. 2** Characterization of device operation in biaxial and uniaxial compression designs. A Schematic of PNIPAM hydrogel devices, with circular and rectangular microcavities to hold cultured tissues. B Devices and microcavities shrink upon incubation. Measurements of C circular and D rectangular microcavity dimensions at room temperature (expanded) and after 24 h incubation (compact). Dashed lines indicate original mold dimensions. (Data in C presented as mean ± standard deviation; $n$ = 38–44 samples; ***$p < 0.001$ by Welch's $t$-test. Data in D presented as mean ± standard deviation; $n$ = 9; **$p < 0.01$ by Wilcoxon matched-pairs signed-rank test).

dynamic range (ESI† Fig. S1). Alternatively, varying the amount of crosslinker or nanoscale gel architecture may be a useful strategy to achieve more broadly tunable compaction ratios.[33,34]

Given the robust shrinkage ratios observed, this approach can hence be applied in principle to generate a wide range of three-dimensional compressive molding fields based on the desired shrunken dimensions of the hydrogel. While the compressive fields generated will be limited by the replica molding cast-and-peel technique which cannot produce fully-enclosed 3D structures, replicating overhanging features[27] can partly ameliorate this concern by enabling fabrication of CHyMs with partially enclosed cavities. We note that while this might permit out-of-plane deformation of the cultured tissue, microcavities could be designed sufficiently deep to allow this deformation to occur without issue. Feature dimensions however will always be limited by 3D print resolution of molds and the fidelity of the hydrogel replica-molding process. While this may hence require some process optimization, the dimensions demonstrated here are sufficient for a wide variety of spheroid and organoid applications.

### Elastic and plastic tissue deformation in CHyM-compacted tissues

As a first demonstration of the tissue molding operation, cancer spheroids were formed in spherical micropocket devices using a previously established protocol,[27] loaded into the cylindrical and rectangular CHyM devices, and compressed for up to 24 hours (Fig. 3A and D). Tissue compaction was rapid and plateaued within 4 hours at radial compression levels of ~50% (Fig. 3B). Although considerable, these compaction levels are not surprising given our previous findings of significant internal spaces within spheroids formed using this technique.[26,35] Once the CHyMs were expanded and the tissues released, they did slightly increase in size within 30 minutes, but then remained in a compacted state for at least 3 hours (Fig. 3C), demonstrating that the spheroid had been both plastically and elastically deformed during compression. Similar results were observed when measuring aspect ratio of spheroids placed under uniaxial compression, where a small amount of elastic recoil was observed after releasing the tissue from compression (Fig. 3D and E). In all cases, cell viability remained high after

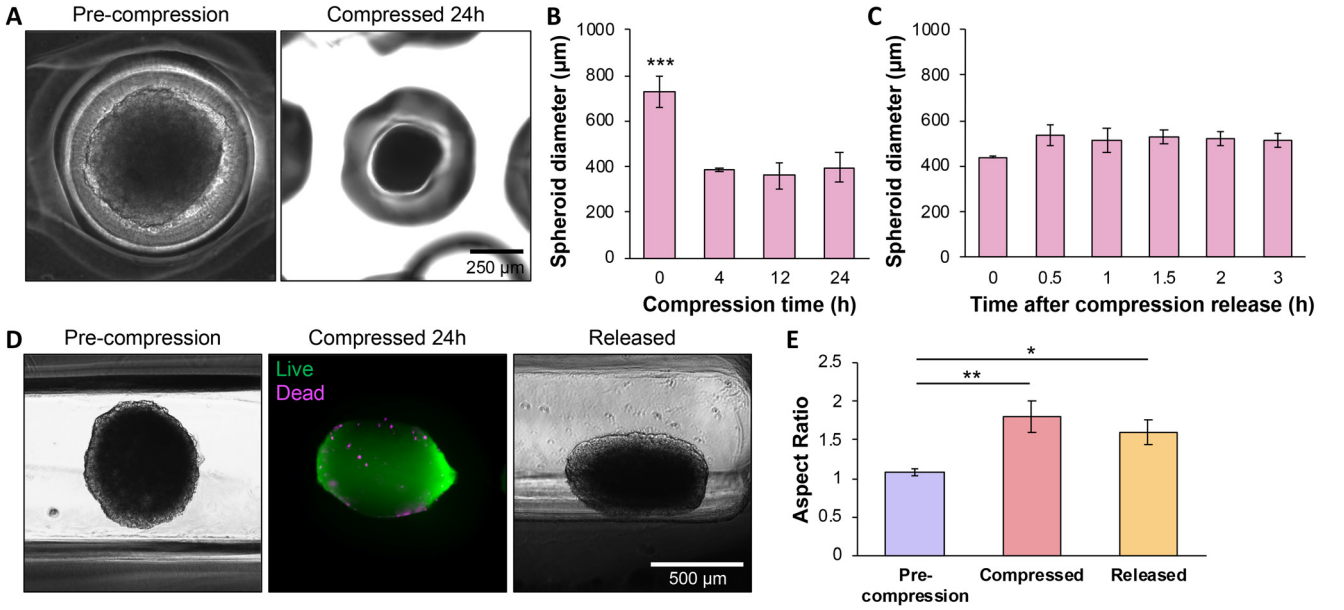


**Fig. 3** Spheroid compression and release with simple shapes. A A T47D spheroid loaded into a room temperature (expanded) circular microcavity, and after 24 h of incubation. B Spheroid diameter during incubation (data presented as mean ± standard deviation; $n$ = 5–22; ***$p < 0.001$ by Welch's ANOVA with Games–Howell *post hoc* test). C Spheroid diameter after addition of chilled media to expand devices and release spheroids from compression (data presented as mean ± standard deviation; $n$ = 3; $p = 0.1686$ by Kruskal–Wallis test). D A T47D spheroid loaded into a room temperature (expanded) rectangular microcavity, after 24 h of incubation with live/dead staining, and after fixing and release (device is expanded). E Measurements of aspect ratio upon loading into rectangular microcavities, after 24 h incubation, and after fixing (data presented as mean ± standard deviation; $n$ = 3–6; *$p < 0.05$, **$p < 0.01$ by Welch's ANOVA with Games–Howell *post hoc* test).

the compaction process (Fig. 3D and S2† for comparison to polyacrylamide, agarose).

### Ring-like brain organoid molding

Since tissues often form tube-like structures such as gut or neural tubes,[36–38] we next demonstrate the potential utility of this platform by molding organoids into ring-like building blocks, that may ultimately be used to generate tube-like structures *via* downstream bioprinting.[6] We therefore designed CHyMs with ring-shaped microcavities (Fig. 4A). This more complex shape was reproducible during device fabrication, and demonstrated similar well-controlled and repeatable shrinkage properties as those observed in the uniaxial and biaxial compression devices. Both the cavity space and the central post of the ring shrank upon incubation, and several cavity/post dimension combinations were tested to illustrate the range of possibilities achievable (Fig. 4B and C). Based on the anticipated size of early-stage brain organoids and their growth rates at the time of molding,[39] CHyM devices with 500 μm cavities and 0.75 mm posts were selected and used in all subsequent experiments. These molds produced structures with an expanded diameter of ~1.7 mm, shrinking to ~0.9 mm when compact, which should allow the organoid to wrap around the central pillar over one week in the CHyM.

During brain organoid formation, many protocols suggest encapsulating the organoid in an extracellular matrix approximately 7 days after the initial formation of the embryoid body. We found that the extracellular matrix Matrigel could be readily incorporated into contracted CHyM devices after initial organoid compression (Fig. 5A). The initial compression of the mold only slightly deformed the brain organoid, which then grew within the compressed cavity to wrap around the central post and reproducibly form a bridge with itself over ~6 days of growth (Fig. 5A; schematic in Fig. 5C). Interestingly, only those organoids encapsulated in Matrigel fused around the central pillar to form rings (Fig. 5B), while organoids that were not encapsulated in Matrigel generally formed a simple elongated organoid adjacent to the central pillar (representative image in Fig. 5D). Similar results were observed when organoids were loaded into CHyMs on days 7–11 after organoid seeding.

In contrast with the previous short-term tissue deformation experiments, these molding experiments were longer and required growth of the tissue into the confining mold chamber, after the initial molding stress was applied. Hence, although this is a combination of both compressive and growth-molding processes, dynamically changing the volume of the culture chamber reduced the length of time required to fill the ring-shaped cavity, and also facilitated release after compression for downstream processing and imaging.

 

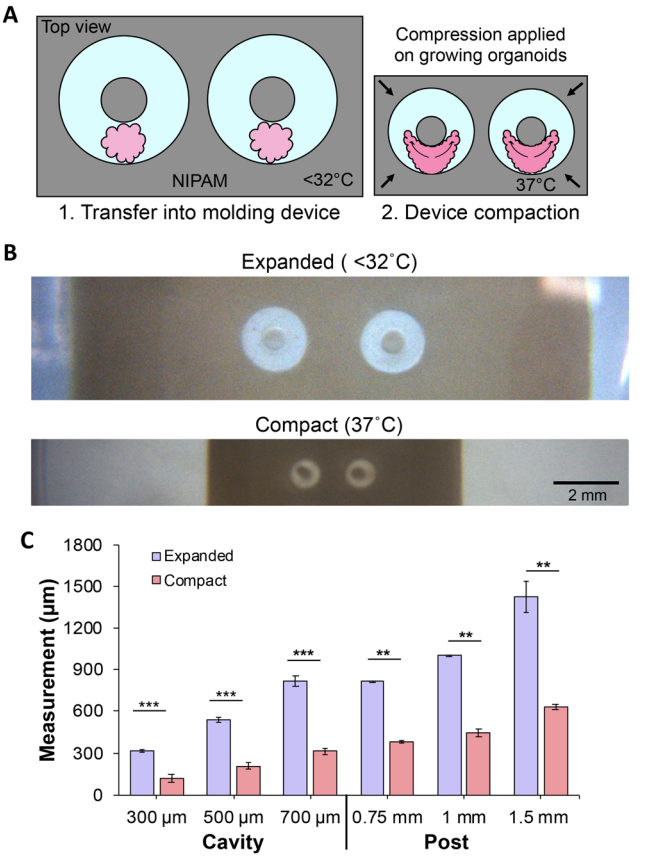


**Fig. 4** Characterization of ring molding devices. A Schematic of PNIPAM hydrogel device with ring-shaped microcavities to guide organoids to adopt ring-like morphologies. B Devices and ring microcavities shrink upon incubation. C Measurements of various microcavity widths and post diameters at room temperature (expanded) and after 24 h incubation (compact) (data presented as mean ± standard deviation; $n$ = 5–10; $^{**}p < 0.01$, $^{***}p < 0.001$ by Wilcoxon signed-rank test).

Throughout this process, the organoid was maintained within a compacted hydrogel structure which may limit diffusion of nutrients and waste. We therefore wanted to confirm that the CHyM did not affect the biological function of the tissue. We first verified that organoids remained viable after 6 days within the CHyM (ESI† Fig. S3), suggesting that sufficient nutrient and oxygen exchange was occurring. We then examined differentiation markers known to characteristically change during this stage of brain organoid culture. At early stages of brain organoid development, tissues strongly express E-cadherin, which is replaced with N-cadherin as differentiation progresses.[40–42] We first confirmed that organoids showed high levels of E-cadherin expression prior to loading them into the CHyM devices (ESI† Fig. S4). Then, after growth and removal from the CHyM device, E-cadherin expression was minimal, while substantial N-cadherin was observed (Fig. 5B). This switch in cadherin expression is consistent with expected progression of cells in this differentiation process, and strongly indicative of appropriate stem cell differentiation. Hence, extended culture in CHyMs did not affect the differentiation program of cells, suggesting that the CHyM system may be useful in both short- and long-term compressive molding applications.

While the applications demonstrated in this paper are in shaping microtissues *via* compressive molding, we believe this platform might be of future importance in investigating fundamental and applied questions in tissue biomechanics and mechanobiology. For example, this platform provides the basis with which to apply spatially-directed compressive forces on developing tissues, which could be used to understand the biophysical cues that drive tumour metastasis, and other mechanically-related diseases.[43–47] Controlled tissue deformation could be used to measure both mechanical plasticity and recovery, and this information could be used to characterize complex tissue mechanics.[46–49] Such platforms could also be used to recreate the various external stresses present during 3D tissue morphogenesis, the process by which tissues, organs, and whole organisms are shaped.[46,50–52] Given several recent studies demonstrating the clear importance of shape-driven mechanical forces on tissue development in tissues as diverse as the pancreas,[53] placenta,[54] lung,[55,56] kidney,[57] mammary gland,[58,59] heart,[37,60] embryonic germ layers,[46,61] and neural tissues,[41,62–65] we believe that the ability to apply 3D deformations to tissues on demand could serve as both a fundamental discovery tool to understand the immediate impact of forces on biological function, as well as an applied strategy to produce shaped tissues of interest.

## Conclusions

We have developed a novel platform utilizing the smart hydrogel PNIPAM to compressively mold microscale tissues such as spheroids and organoids in a standard cell culture incubator. The geometry of the replica-molded microcavities can be designed in a variety of simple or complex shapes, and can be used to apply selected compressive profiles to tissues in culture. The CHyM platform makes it possible to start with uncontrolled and randomly shaped spheroids and organoids, thus enabling integration with existing spheroid/organoid generation methods, and *via* compressive molding to produce tissues with morphologies as desired. This technology could be applied to shape building blocks for bioassembly to create larger and more complex tissue constructs containing multiple tissue types, combining advantages of organoid cultures and bioprinting. This would yield more realistic and functional synthetic organs, and could also facilitate developmental studies in systems with various interacting components.

## Conflicts of interest

There are no conflicts of interest to declare.

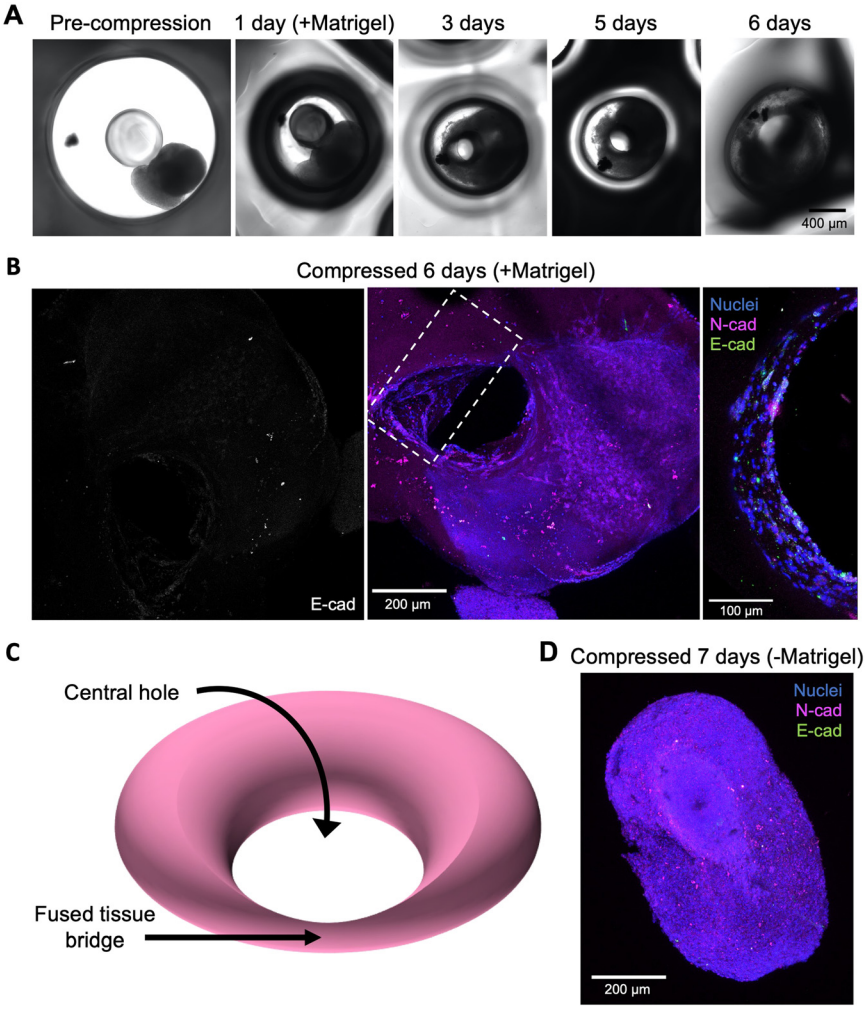


**Fig. 5** Organoid molding in ring CHyMs. A A brain organoid loaded into a room temperature (expanded) ring microcavity, and over 6 days of growth in the device. B Staining of the ring organoid after 6 days of CHyM compression with closeup of the point of fusion (approximate location outlined in white box) shows dominant N-cadherin (N-cad) and minimal E-cadherin (E-cad) expression. C Schematic of an organoid that formed a ring around the central pillar of the CHyM, fusing with itself to form a bridge. D Organoids cultured in CHyMs without Matrigel did not form rings.

## Acknowledgements

We thank Professor Timothy E Kennedy and Melissa Pestemalciyan for generous assistance with antibodies and staining; Meghna Mathur for support with iPSC culture; María Lacalle-Aurioles for use of her imaging chamber; Benjamin E Campbell for his spheroid devices; Christina-Marie Boghdady for use of her device molds; and the Neuro Microscopy Imaging Centre. This work was supported by funding received from the CQDM Quantum Leaps program and the Canada First Research Excellence Fund, awarded through the Healthy Brains, Healthy Lives initiative at McGill University to TMD and CM, and the NSERC Discovery (RGPIN-2022-05165) to CM. We gratefully acknowledge personnel support from the Healthy Brains, Healthy Lives program, and the NSERC Postgraduate Scholarship-Doctoral to CCC and SM, and the Canada Research Chairs in Advanced Cellular Microenvironments to CM.

## References

1 L. Moroni, T. Boland, J. A. Burdick, C. De Maria, B. Derby, G. Forgacs, J. Groll, Q. Li, J. Malda, V. A. Mironov, C. Mota, M. Nakamura, W. Shu, S. Takeuchi, T. B. F. Woodfield, T. Xu, J. J. Yoo and G. Vozzi, Biofabrication: A Guide to Technology and Terminology, *Trends Biotechnol.*, 2018, 384–402, DOI: **10.1016/j.tibtech.2017.10.015**.

2 K. Ino, F. Ozawa, N. Dang, K. Hiramoto, S. Hino, R. Akasaka, Y. Nashimoto and H. Shiku, Biofabrication Using Electrochemical Devices and Systems, *Adv. Biosyst.*, 2020, **4**(4), 1900234, DOI: **10.1002/ADBI.201900234**.

3 P. Bajaj, R. M. Schweller, A. Khademhosseini, J. L. West and R. Bashir, 3D Biofabrication Strategies for Tissue Engineering and Regenerative Medicine, *Annu. Rev. Biomed. Eng.*, 2014, **16**, 247, DOI: **10.1146/ANNUREV-BIOENG-071813-105155**.

4 M. Castilho, M. de Ruijter, S. Beirne, C. C. Villette, K. Ito, G. G. Wallace and J. Malda, Multitechnology Biofabrication:

 

A New Approach for the Manufacturing of Functional Tissue Structures?, *Trends Biotechnol.*, 2020, 1316–1328, DOI: 10.1016/j.tibtech.2020.04.014.

5 P. Bajaj, X. Tang, T. A. Saif and R. Bashir, Stiffness of the Substrate Influences the Phenotype of Embryonic Chicken Cardiac Myocytes, *J. Biomed. Mater. Res., Part A*, 2010, **95**(4), 1261–1269, DOI: 10.1002/jbm.a.32951.

6 J. A. Brassard, M. Nikolaev, T. Hübscher, M. Hofer and M. P. Lutolf, Recapitulating Macro-Scale Tissue Self-Organization through Organoid Bioprinting, *Nat. Mater.*, 2021, **20**(1), 22–29, DOI: 10.1038/s41563-020-00803-5.

7 M. A. Skylar-Scott, S. G. M. Uzel, L. L. Nam, J. H. Ahrens, R. L. Truby, S. Damaraju and J. A. Lewis, Biomanufacturing of Organ-Specific Tissues with High Cellular Density and Embedded Vascular Channels, *Sci. Adv.*, 2019, **5**(9), DOI: 10.1126/sciadv.aaw2459.

8 M. A. Lancaster and J. A. Knoblich, Generation of Cerebral Organoids from Human Pluripotent Stem Cells, *Nat. Protoc.*, 2014, **9**(10), 2329–2340, DOI: 10.1038/nprot.2014.158. Generation.

9 T. Sato, R. G. Vries, H. J. Snippert, M. Van De Wetering, N. Barker, D. E. Stange, J. H. Van Es, A. Abo, P. Kujala, P. J. Peters and H. Clevers, Single Lgr5 Stem Cells Build Crypt-Villus Structures in Vitro without a Mesenchymal Niche, *Nature*, 2009, **459**(7244), 262–265, DOI: 10.1038/nature07935.

10 N. Sachs, Y. Tsukamoto, P. Kujala, P. J. Peters and H. Clevers, Intestinal Epithelial Organoids Fuse to Form Self-Organizing Tubes in Floating Collagen Gels, *Dev.*, 2017, **144**(6), 1107–1112, DOI: 10.1242/DEV.143933/VIDEO-2.

11 J. A. Reid, P. A. Mollica, R. D. Bruno and P. C. Sachs, Consistent and Reproducible Cultures of Large-Scale 3D Mammary Epithelial Structures Using an Accessible Bioprinting Platform, *Breast Cancer Res.*, 2018, **20**(1), 1–13, DOI: 10.1186/s13058-018-1069-9.

12 Y. Miura, M. Y. Li, F. Birey, K. Ikeda, O. Revah, M. V. Thete, J. Y. Park, A. Puno, S. H. Lee, M. H. Porteus and S. P. Paşca, Generation of Human Striatal Organoids and Cortico-Striatal Assembloids from Human Pluripotent Stem Cells, *Nat. Biotechnol.*, 2020, **38**(12), 1421–1430, DOI: 10.1038/s41587-020-00763-w.

13 Y. Miura, M. Y. Li, O. Revah, S. J. Yoon, G. Narazaki and S. P. Paşca, Engineering Brain Assembloids to Interrogate Human Neural Circuits, *Nat. Protoc.*, 2022, **17**(1), 15–35, DOI: 10.1038/s41596-021-00632-z.

14 G. Martínez-Ara, K. S. Stapornwongkul and M. Ebisuya, Scaling up Complexity in Synthetic Developmental Biology, *Science*, 2022, **378**(6622), 864–868, DOI: 10.1126/SCIENCE.ADD9666.

15 E. Karzbrun, A. Kshirsagar, S. R. Cohen, J. H. Hanna and O. Reiner, Human Brain Organoids on a Chip Reveal the Physics of Folding, *Nat. Phys.*, 2018, **14**(5), 515–522, DOI: 10.1038/s41567-018-0046-7.

16 S. E. Park, S. Kang, J. Paek, A. Georgescu, J. Chang, A. Y. Yi, B. J. Wilkins, T. A. Karakasheva, K. E. Hamilton and D. D. Huh, Geometric Engineering of Organoid Culture for Enhanced Organogenesis in a Dish, *Nat. Methods*, 2022, **19**(November), 1449–1460, DOI: 10.1038/s41592-022-01643-8.

17 M. A. Lancaster, N. S. Corsini, S. Wolfinger, E. H. Gustafson, A. W. Phillips, T. R. Burkard, T. Otani, F. J. Livesey and J. A. Knoblich, Guided Self-Organization and Cortical Plate Formation in Human Brain Organoids, *Nat. Biotechnol.*, 2017, **35**(7), 659–666, DOI: 10.1038/nbt.3906.

18 N. N. Ferreira, L. M. B. Ferreira, V. M. O. Cardoso, F. I. Boni, A. L. R. Souza and M. P. D. Gremião, Recent Advances in Smart Hydrogels for Biomedical Applications: From Self-Assembly to Functional Approaches, *Eur. Polym. J.*, 2018, **99**(November 2017), 117–133, DOI: 10.1016/j.eurpolymj.2017.12.004.

19 V. A. B. Quiñones, H. Zhu, A. A. Solovev, Y. Mei and D. H. Gracias, Origami Biosystems: 3D Assembly Methods for Biomedical Applications, *Adv. Biosyst.*, 2018, **2**(12), 1800230, DOI: 10.1002/ADBI.201800230.

20 J. Shang, X. Le, J. Zhang, T. Chen and P. Theato, Trends in Polymeric Shape Memory Hydrogels and Hydrogel Actuators, *Polym. Chem.*, 2019, **10**(9), 1036–1055, DOI: 10.1039/C8PY01286E.

21 F. M. Cheng, H. X. Chen and H. D. Li, Recent Progress on Hydrogel Actuators, *J. Mater. Chem. B*, 2021, **9**(7), 1762–1780, DOI: 10.1039/D0TB02524K.

22 E. J. Choi, S. Ha, J. Lee, T. Premkumar and C. Song, UV-Mediated Synthesis of PNIPAM-Crosslinked Double-Network Alginate Hydrogels: Enhanced Mechanical and Shape-Memory Properties by Metal Ions and Temperature, *Polymer*, 2018, **149**, 206–212, DOI: 10.1016/J.POLYMER.2018.06.080.

23 R. Luo, J. Wu, N. D. Dinh and C. H. Chen, Gradient Porous Elastic Hydrogels with Shape-Memory Property and Anisotropic Responses for Programmable Locomotion, *Adv. Funct. Mater.*, 2015, **25**(47), 7272–7279, DOI: 10.1002/ADFM.201503434.

24 A. Romo-Uribe and L. Albanil, POSS-Induced Dynamic Cross-Links Produced Self-Healing and Shape Memory Physical Hydrogels When Copolymerized with N-Isopropyl Acrylamide, *ACS Appl. Mater. Interfaces*, 2019, **11**(27), 24447–24458, DOI: 10.1021/acsami.9b06672.

25 A. Halperin, M. Kröger and F. M. Winnik, Poly(N-Isopropylacrylamide) Phase Diagrams: Fifty Years of Research, *Angew. Chem., Int. Ed.*, 2015, **54**(51), 15342–15367, DOI: 10.1002/anie.201506663.

26 S. Mok, S. Al Habyan, C. Ledoux, W. Lee, K. N. MacDonald, L. McCaffrey and C. Moraes, Mapping Cellular-Scale Internal Mechanics in 3D Tissues with Thermally Responsive Hydrogel Probes, *Nat. Commun.*, 2020, **11**(1), 1–11, DOI: 10.1038/s41467-020-18469-7.

27 L. Zhao, S. Mok and C. Moraes, Micropocket Hydrogel Devices for All-in-One Formation, Assembly, and Analysis of Aggregate-Based Tissues, *Biofabrication*, 2019, **11**(4), 045013, DOI: 10.1088/1758-5090/ab30b4.

28 C. X. Q. Chen, N. Abdian, G. Maussion, R. A. Thomas, I. Demirova, E. Cai, M. Tabatabaei, L. K. Beitel, J. Karamchandani, E. A. Fon and T. M. Durcan, A Multistep Workflow to Evaluate Newly Generated Ipscs and Their

Ability to Generate Different Cell Types, *Methods Protoc.*, 2021, **4**(3), 50, DOI: **10.3390/MPS4030050/S1**.

29 N.-V. Mohamed, M. Mathur, R. V. da Silva, R. A. Thomas, P. Lepine, L. K. Beitel, E. A. Fon and T. M. Durcan, Generation of Human Midbrain Organoids from Induced Pluripotent Stem Cells, *MNI Open Res.*, 2021, **3**, 1, DOI: **10.12688/mniopenres.12816.2**.

30 J. Schindelin, I. Arganda-Carreras, E. Frise, V. Kaynig, M. Longair, T. Pietzsch, S. Preibisch, C. Rueden, S. Saalfeld, B. Schmid, J. Y. Tinevez, D. J. White, V. Hartenstein, K. Eliceiri, P. Tomancak and A. Cardona, Fiji: An Open-Source Platform for Biological-Image Analysis, *Nat. Methods*, 2012, 676–682, DOI: **10.1038/nmeth.2019**.

31 S. Preibisch, S. Saalfeld and P. Tomancak, Globally Optimal Stitching of Tiled 3D Microscopic Image Acquisitions, *Bioinformatics*, 2009, **25**(11), 1463–1465, DOI: **10.1093/BIOINFORMATICS/BTP184**.

32 R Core Team, *R: A Language and Environment for Statistical Computing*, R Foundation for Statistical Computing, Vienna, Austria, 2017.

33 T. Okajima, I. Harada, K. Nishio and S. Hirotsu, Kinetics of Volume Phase Transition in Poly(N-Isopropylacrylamide) Gels, *J. Chem. Phys.*, 2002, **116**(20), 9068–9077, DOI: **10.1063/1.1473655**.

34 L. W. Xia, R. Xie, X. J. Ju, W. Wang, Q. Chen and L. Y. Chu, Nano-Structured Smart Hydrogels with Rapid Response and High Elasticity, *Nat. Commun.*, 2013, **4**(1), 1–11, DOI: **10.1038/ncomms3226**.

35 W. Lee, N. Kalashnikov, S. Mok, R. Halaoui, E. Kuzmin, A. J. Putnam, S. Takayama, M. Park, L. McCaffrey, R. Zhao, R. L. Leask and C. Moraes, Dispersible Hydrogel Force Sensors Reveal Patterns of Solid Mechanical Stress in Multicellular Spheroid Cultures, *Nat. Commun.*, 2019, **10**(1), 1–14, DOI: **10.1038/s41467-018-07967-4**.

36 B. Lubarsky and M. A. Krasnow, Tube Morphogenesis: Making and Shaping Biological Tubes, *Cell*, 2003, **112**, 19–28.

37 L. A. Taber, Morphomechanics: Transforming Tubes into Organs, *Curr. Opin. Genet. Dev.*, 2014, **27**(Ic), 7–13, DOI: **10.1016/j.gde.2014.03.004**.

38 M. Tozluoğlu and Y. Mao, On Folding Morphogenesis, a Mechanical Problem, *Philos. Trans. R. Soc., B*, 2020, **375**(1809), 20190564, DOI: **10.1098/rstb.2019.0564**.

39 C. C. de Camps, S. Aslani, N. Stylianesis, H. Nami, N. V. Mohamed, T. M. Durcan and C. Moraes, Hydrogel Mechanics Influence the Growth and Development of Embedded Brain Organoids, *ACS Appl. Bio Mater.*, 2022, **5**(1), 214–224, DOI: **10.1021/ACSABM.1C01047/SUPPL_FILE/MT1C01047_SI_001.PDF**.

40 M. A. Lancaster, M. Renner, C. A. Martin, D. Wenzel, L. S. Bicknell, M. E. Hurles, T. Homfray, J. M. Penninger, A. P. Jackson and J. A. Knoblich, Cerebral Organoids Model Human Brain Development and Microcephaly, *Nature*, 2013, **501**(7467), 373–379, DOI: **10.1038/nature12517**.

41 E. Karzbrun, A. H. Khankhel, H. C. Megale, S. M. K. Glasauer, Y. Wyle, G. Britton, A. Warmflash, K. S. Kosik, E. D. Siggia, B. I. Shraiman and S. J. Streichan, Human Neural Tube Morphogenesis in Vitro by Geometric Constraints, *Nature*, 2021, **599**(7884), 268–272, DOI: **10.1038/s41586-021-04026-9**.

42 A. Ranga, M. Girgin, A. Meinhardt, D. Eberle, M. Caiazzo, E. M. Tanaka and M. P. Lutolf, Neural Tube Morphogenesis in Synthetic 3D Microenvironments, *Proc. Natl. Acad. Sci. U. S. A.*, 2016, **113**(44), E6831–E6839, DOI: **10.1073/pnas.1603529113**.

43 S. Kumar and V. M. Weaver, Mechanics, Malignancy, and Metastasis: The Force Journey of a Tumor Cell, *Cancer Metastasis Rev.*, 2009, **28**(1–2), 113–127, DOI: **10.1007/S10555-008-9173-4**.

44 M. J. Paszek, N. Zahir, K. R. Johnson, J. N. Lakins, G. I. Rozenberg, A. Gefen, C. A. Reinhart-King, S. S. Margulies, M. Dembo, D. Boettiger, D. A. Hammer and V. M. Weaver, Tensional Homeostasis and the Malignant Phenotype, *Cancer Cell*, 2005, **8**(3), 241–254, DOI: **10.1016/J.CCR.2005.08.010**.

45 Z. Ma, L. Sagrillo-Fagundes, S. Mok, C. Vaillancourt and C. Moraes, Mechanobiological Regulation of Placental Trophoblast Fusion and Function through Extracellular Matrix Rigidity, *Sci. Rep.*, 2020, **10**(1), 5837, DOI: **10.1038/s41598-020-62659-8**.

46 M. K. Hayward, J. M. Muncie and V. M. Weaver, Tissue Mechanics in Stem Cell Fate, Development, and Cancer, *Dev. Cell*, 2021, **56**(13), 1833–1847, DOI: **10.1016/J.DEVCEL.2021.05.011**.

47 C. Ort, W. Lee, N. Kalashnikov and C. Moraes, Disentangling the Fibrous Microenvironment: Designer Culture Models for Improved Drug Discovery, *Expert Opin. Drug Discovery*, 2020, 1–13, DOI: **10.1080/17460441.2020.1822815**.

48 N. Khalilgharibi and Y. Mao, To Form and Function: On the Role of Basement Membrane Mechanics in Tissue Development, Homeostasis and Disease, *Open Biol.*, 2021, **11**(2), DOI: **10.1098/rsob.200360**.

49 D. Grossman and J. F. Joanny, Instabilities and Geometry of Growing Tissues, *Phys. Rev. Lett.*, 2022, **129**(4), DOI: **10.1103/PhysRevLett.129.048102**.

50 G. A. Stooke-Vaughan and O. Campàs, Physical Control of Tissue Morphogenesis across Scales, *Curr. Opin. Genet. Dev.*, 2018, 111–119, DOI: **10.1016/j.gde.2018.09.002**.

51 C.-P. Heisenberg and Y. Bellaïche, Forces in Tissue Morphogenesis and Patterning, *Cell*, 2013, **153**(5), 948–962, DOI: **10.1016/j.cell.2013.05.008**.

52 K. Goodwin and C. M. Nelson, Mechanics of Development, *Dev. Cell*, 2021, **56**(2), 240–250, DOI: **10.1016/J.DEVCEL.2020.11.025**.

53 R. Tran, C. Moraes and C. A. Hoesli, Controlled Clustering Enhances PDX1 and NKX6.1 Expression in Pancreatic Endoderm Cells Derived from Pluripotent Stem Cells, *Sci. Rep.*, 2020, **10**(1), 1190, DOI: **10.1038/s41598-020-57787-0**.

54 Z. Ma, L. Sagrillo-Fagundes, R. Tran, P. K. Parameshwar, N. Kalashnikov, C. Vaillancourt and C. Moraes, Biomimetic Micropatterned Adhesive Surfaces to Mechanobiologically Regulate Placental Trophoblast Fusion, *ACS Appl. Mater.*

 

*Interfaces*, 2019, **11**(51), 47810–47821, DOI: **10.1021/acsami.9b19906**.

55 H. Y. Kim, M. F. Pang, V. D. Varner, L. Kojima, E. Miller, D. C. Radisky and C. M. Nelson, Localized Smooth Muscle Differentiation Is Essential for Epithelial Bifurcation during Branching Morphogenesis of the Mammalian Lung, *Dev. Cell*, 2015, **34**(6), 719–726, DOI: **10.1016/j.devcel.2015.08.012**.

56 K. Goodwin, S. Mao, T. Guyomar, E. Miller, D. C. Radisky, A. Košmrlj and C. M. Nelson, Smooth Muscle Differentiation Shapes Domain Branches during Mouse Lung Development, *Development*, 2019, **146**(22), dev181172, DOI: **10.1242/dev.181172**.

57 C. M. Nelson, J. L. Inman and M. J. Bissell, Three-Dimensional Lithographically Defined Organotypic Tissue Arrays for Quantitative Analysis of Morphogenesis and Neoplastic Progression, *Nat. Protoc.*, 2008, **3**(4), 674–678, DOI: **10.1038/nprot.2008.35**.

58 C. M. Nelson, M. M. VanDuijn, J. L. Inman, D. A. Fletcher and M. J. Bissell, Tissue Geometry Determines Sites of Mammary Branching Morphogenesis in Organotypic Cultures, *Science*, 2006, **314**(5797), 298, DOI: **10.1126/SCIENCE.1131000**.

59 N. Gjorevski and C. M. Nelson, Endogenous Patterns of Mechanical Stress Are Required for Branching Morphogenesis, *Integr. Biol.*, 2010, **2**(9), 424–434, DOI: **10.1039/C0IB00040J**.

60 C. J. Mandrycky, N. P. Williams, I. Batalov, D. El-Nachef, B. de Bakker, J. Davis, D. H. Kim, C. A. DeForest, Y. Zheng, K. R. Stevens and N. J. Sniadecki, Engineering Heart Morphogenesis, *Trends Biotechnol.*, 2020, **38**(8), 835–845, DOI: **10.1016/j.tibtech.2020.01.006**.

61 A. Warmflash, B. Sorre, F. Etoc, E. D. Siggia and A. H. Brivanlou, A Method to Recapitulate Early Embryonic Spatial Patterning in Human Embryonic Stem Cells, *Nat. Methods*, 2014, **11**(8), 847–854, DOI: **10.1038/nmeth.3016**.

62 E. Nikolopoulou, G. L. Galea, A. Rolo, N. D. E. Greene and A. J. Copp, Neural Tube Closure: Cellular, Molecular and Biomechanical Mechanisms, *Dev.*, 2017, **144**(4), 552–566, DOI: **10.1242/dev.145904**.

63 X. Xue, Y. Sun, A. M. Resto-Irizarry, Y. Yuan, K. M. A. Yong, Y. Zheng, S. Weng, Y. Shao, Y. Chai, L. Studer and J. Fu, Mechanics-Guided Embryonic Patterning of Neuroectoderm Tissue from Human Pluripotent Stem Cells, *Nat. Mater.*, 2018, **17**(7), 633–641, DOI: **10.1038/s41563-018-0082-9**.

64 G. T. Knight, B. F. Lundin, N. Iyer, L. M. T. Ashton, W. A. Sethares, R. M. Willett and R. S. Ashton, Engineering Induction of Singular Neural Rosette Emergence within HPSC-Derived Tissues, *eLife*, 2018, **7**, e37549, DOI: **10.7554/eLife.37549**.

65 T. Haremaki, J. J. Metzger, T. Rito, M. Z. Ozair, F. Etoc and A. H. Brivanlou, Self-Organizing Neuruloids Model Developmental Aspects of Huntington's Disease in the Ectodermal Compartment, *Nat. Biotechnol.*, 2019, **37**(10), 1198–1208, DOI: **10.1038/s41587-019-0237-5**.